Physica B: Physics of Condensed Matter 528 (2018) 60–65

Contents lists available at ScienceDirect

Physica B: Physics of Condensed Matter

journal homepage: www.elsevier.com/locate/physb

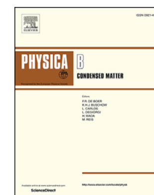

# Properties of transparent conducting tin monoxide(SnO) thin films prepared by chemical spray pyrolysis method

Ebitha Eqbal, E.I. Anila *

*Optoelectronic and Nanomaterials' Research Laboratory, Department of Physics, Union Christian College, Aluva, Kerala, 683102, India*

ARTICLE INFO

*Keywords:*
Thin film
Spray pyrolysis
Orthorhombic
Ellipsometry
Chromaticity coordinates

ABSTRACT

Transparent conducting Stannous Oxide (SnO) thin films were obtained by chemical spray pyrolysis method on glass substrates for 0.1 M and 0.25 M concentration of precursor solutions. Their structural, morphological, optical and electrical properties were investigated. X-ray diffraction (XRD) study shows polycrystalline nature of the films with orthorhombic crystal structure. The morphological analysis was carried out by Scanning electron microscopy (SEM) and elemental analysis was done by Energy dispersive X-ray spectroscopy (EDX). The band gap of 0.1 M and 0.25 M thin film samples were found to be 3.58eV with 82% transmission and 3 eV with 30% transmission respectively. The film thickness, refractive index (n) and extinction coefficient (k) of the films were obtained by ellipsometric technique. Hall effect measurements reveal p-type conduction with mobility 7.8 $cm^2V^{-1}s^{-1}$ and 15 $cm^2V^{-1}s^{-1}$ and conductivity of 8.5 S/cm and 17.1 S/cm respectively for the 0.1 M and 0.25 M samples. Photoluminescence (PL) spectrum of the samples show a broad emission which covers near band edge (NBE) as well as deep level emission (DLE) in the region 380 nm-620 nm.

## 1. Introduction

Transparent Conducting oxides (TCOs) are widely used in various opto electronic applications like low emission glass, electrodes, organic light emitting diodes, lithium batteries, gas sensors, heat reflectors, polymer based electronics, flat panel displays, solar cells etc [1–8]. Generally TCOs are n-type semiconductors, high quality p-type conducting TCOs remains few. Because of that the field of application of oxide semiconductors reduces to unipolar devices.

Due to native p-type conductivity and stability in maintaining both structure and electronic properties Stannous oxide (SnO) has been attracted significant attention [9]. SnO could serve as a better native p-type oxide semiconductor because of the energy level of Sn 5s is closer to that of O 2p near the valence band maximum (VBM) and Sn 5p near the conduction band, thus allowing for a more effective reduction of hole localization along with high hole mobility. The origin of p-type conductivity of SnO is mainly due to Sn vacancies and oxygen interstitials [10]. SnO processes wide band gap ranging from 2.5 to 3.4 eV [9,11] and excellent p-type behaviour, applicable for many opto electronic devices including heterojunction diodes, TFT's and complementary circuits and other applications like gas sensitive material, catalyst, precursor for the production of tin dioxide($SnO_2$) [12–17]. Recently Jesus A. Caraveo-Frescast et al. reported record hole mobility of 18.71 $cm^2/V$ s in SnO thin films and fabricated thin film transistors by physical vapour deposition [18].

Various techniques such as electron beam evaporation [17], magnetron sputtering [19], sol-gel [20], atomic layer deposition [21], pulsed laser deposition [22] etc. are used for the deposition of SnO thin films, but a very few have reported spray pyrolysis [23] deposition of SnO thin films. Since SnO is easily oxidized and becomes unstable, preparation of p-type SnO thin film is challenging. In this study, we are reporting p-type SnO thin film for 0.1 M and 0.25 M concentration of precursor solution using chemical spray pyrolysis at 350 °C. We also tried for other molarities, for that we got n-type Stannic Oxide ($SnO_2$). The structural, compositional, optical, electrical and morphological properties of the prepared films were comprehensively investigated. To best of our knowledge, this is the first time report of ellipsometric studies of SnO thin film by chemical spray pyrolysis method.

## 2. Experimental

An amount of required grams of $SnCl_2{\cdot}2H_2O$ was dissolved in distilled water to make 0.1 M and 0.25 M precursor solutions and a few drops of concentrated hydrochloric acid was added to make the solution transparent. Then the mixture was magnetically stirred at 60 °C for an hour. Glass slides were used as substrates on which films grown. Ultrasonically

* Corresponding author.
*E-mail address:* anilaei@gmail.com (E.I. Anila).

https://doi.org/10.1016/j.physb.2017.10.080
Received 22 June 2017; Received in revised form 17 October 2017; Accepted 18 October 2017
Available online 22 October 2017
0921-4526/© 2017 Elsevier B.V. All rights reserved.

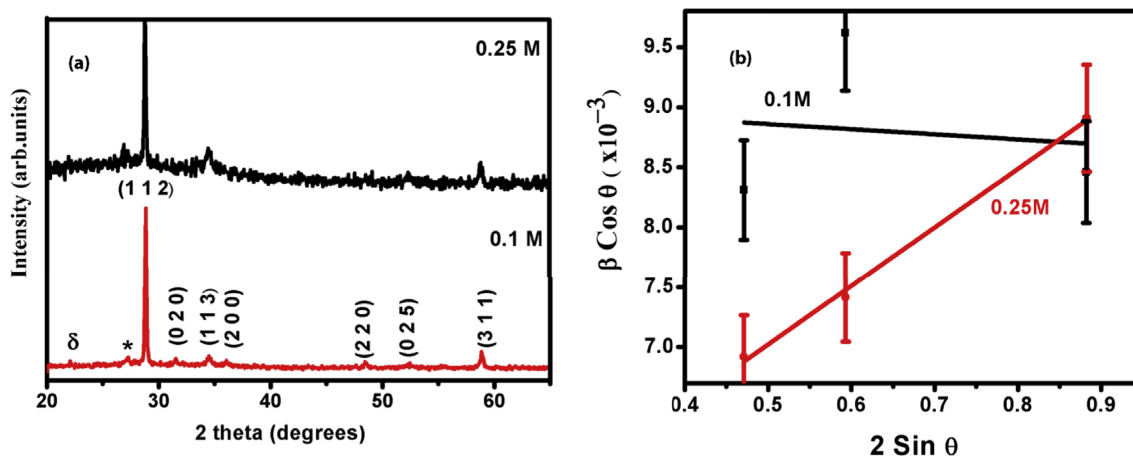


**Fig. 1.** (a) XRD diagram and (b) W-H Plot fitted with major peaks of SnO thin films for 0.1 M and 0.25 M concentration of precursor solutions. The "*" sign denotes the $SnO_2$ phase coming along with SnO during preparation, and "δ" sign denotes the unidentified peak.

cleaned substrates were placed on the substrate heater of the spray equipment to provide proper heating with uniformity to films. Spraying was done at a substrate temperature of 350° C. The substrates were removed immediately after spraying and allowed to cool at room temperature.

The structural characterization of the SnO thin films were carried out using XRD and X-ray diffraction data were recorded on a Rigaku D-Max Geigerflex X-ray diffractometer using CuKα radiation source ($\lambda = 1.5418$ Å) for 2θ values between 20° and 80° at room temperature. The morphology and microstructure of the prepared films were studied by Scanning electron microscopy (SEM) using JEOL JSM 7600F field emission scanning electron microscope. Elemental characterization of prepared films was done by Energy Dispersive X-ray spectrometer (EDX) using JEOL JSM 6390 LV. The optical characterization of the SnO thin films were studied by using Shimadzu UV–Vis spectrophotometer model-UV 1800. PL studies were carried out using Fluoromax-4 spectrofluorometer. The thickness of the films were measured using ellipsometric technique using J.A.Woolam Co. Inc M 2000 ellipsometer. The electrical characterization was done using Hall effect measurements using ECOPIA HMS-5000 in Vander Pauw configuration.

## 3. Results and discussion

### 3.1. Structural analysis

Tin monoxides mainly have three types of crystal structures: tetragonal SnO (α-SnO), orthorhombic SnO (O-SnO), and β-SnO. To determine the crystal structure of the films X-ray diffraction technique is employed. The XRD pattern of SnO thin films is shown in Fig. 1(a). The grown SnO have exhibited strong orientation along (112) plane and also other peaks along (020), (113), (200), (220), (025), (311) can be seen which are in agreement with the standard JCPDS file no: 77-2296, having orthorhombic crystal structure(O-SnO). A small percentage of $SnO_2$ phase is also observed in the XRD pattern.

The average grain size of sprayed SnO thin film was calculated using the Debye -Scherrer formula [24],

$$D = 0.9\lambda/\beta \cos\theta$$

where λ is the wavelength of X-ray radiations, β is the full width at half maximum of the diffraction peak, and θ is the glancing angle. From Debye Scherrer formula, the grain size of the samples were found to increase with molarity with values 15.80 nm (0.1 M) and 31.55 nm (0.25 M). The diffraction line broadening caused by the strain and reduced grain size was analyzed using the Williamson–Hall (W–H) method. The W–H plots for SnO thin films are depicted in Fig. 1(b).

The relation used for the calculation of lattice strain and crystallite size [24–26] is

$$\beta \cos\theta = 0.9\lambda/D + 2\xi \sin\theta,$$

where ξ represents the lattice strain, β is the full width at half maximum of the diffraction peak, and θ is the glancing angle and D is the average grain size calculated using Debye Scherrer formula. The average grain size of SnO thin films calculated from W-H plot are 15.29 nm and

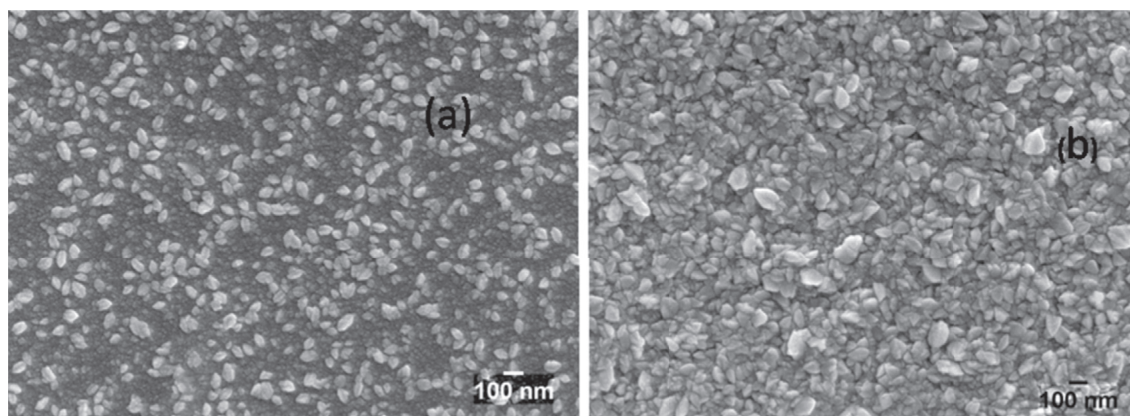


**Fig. 2.** SEM images of SnO thin films for (a) 0.1 M, (b) 0.25 M concentration of precursor solutions.

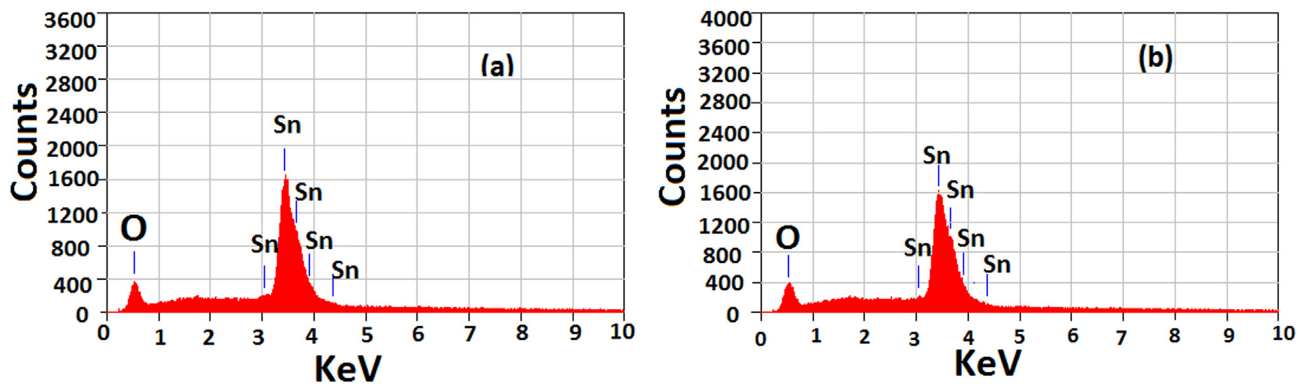


**Fig. 3.** EDX Spectrum of SnO thin films for (a) 0.1 M and (b) 0.25 M concentration of precursor solutions.

28.39 nm respectively for 0.1 M and 0.25 M concentration of precursor solutions. We got small compressive strain for 0.1 M sample with value 0.424 and large elongation strain for 0.25 M sample with value 4.884.

### 3.2. Morphological analysis

The morphological analysis was carried out by SEM. The SEM images of the SnO thin films for different molarities is shown in Fig. 2(a and b) which reveals that the films have smooth and homogeneous surface morphology with small granular grains distributed throughout the surface. There are no cracks seen on the surface of the film and the grain size increases with molarity.

### 3.3. Elemental analysis

Elemental analysis of prepared tin oxide thin films was carried out by EDX. Fig. 3(a and b) represents the EDX spectrum of SnO thin film for 0.1 M and 0.25 M concentration of the precursor solutions respectively. EDX analysis confirms the presence of Sn and O elements in the prepared SnO film. The Sn/O ratio for 0.1 M and 0.25 M samples are found to be 1.16 and 1.21 respectively. This shows the presence of oxygen vacancies in both samples.

### 3.4. Optical properties

The transmission percentage of SnO thin films are 82% for 0.1 M, which was reduced to 30% for 0.25 M concentration of precursor solution as shown in Fig. 4(a). The reduction in transmission percentage may be due to the presence of metallic tin in the film 0.25 M SnO thin film.

The optical band gap was examined using the relation proposed by Tauc, Davis and Mott [24] which relates the absorption coefficient α to the incident photon energy hυ as

$$\alpha h\upsilon = A\left(h\upsilon - E_g\right)^n$$

where hυ is the photon energy,α is the absorbance, A is a constant and n is ½ for direct transition. Fig. 4(b) shows the variation of $(\alpha h\upsilon)^2$ and hυ of SnO thin films. The optical band gap has then been determined by extrapolating the linear portion of the $(\alpha h\upsilon)^2$ curve to zero, obtained values of band gaps are 3.58 eV for 0.1 M, which was reduced to 3 eV for 0.25 M concentration of precursor solutions of SnO thin films. The decrease in band gap with molarity is due to the presence of defects and metallic tin present in the sample. There are reports of 3.8 eV for SnO nanoparticles in the strong confinement regime [27].

### 3.5. Photoluminescence studies

Fig. 5(a) shows the room-temperature photoluminescence spectra collected by using an excitation wavelength of 335 nm. Photoluminescence (PL) spectrum of the samples show a broad emission which covers near band edge (NBE) as well as deep level emission (DLE) in the region 380 nm-620 nm. From the figure it was observed that there are two broad emissions for SnO at 0.1 M concentration of precursor solution with two main peaks, one at 407 nm and the other at 517 nm. While peak at 407 nm corresponds to near band edge emission (NBE) of SnO, peak at 517 nm can be attributed to deep level emission (DLE). For 0.25 M sample a broad emission was obtained which is deconvoluted to NBE emission at 413 nm and DLE emission at 520 nm.The red shift in emission peaks is due to the red shift in band gap of 0.25 M sample with respect to 0.1 M sample. From EDX study we observed that, for both samples

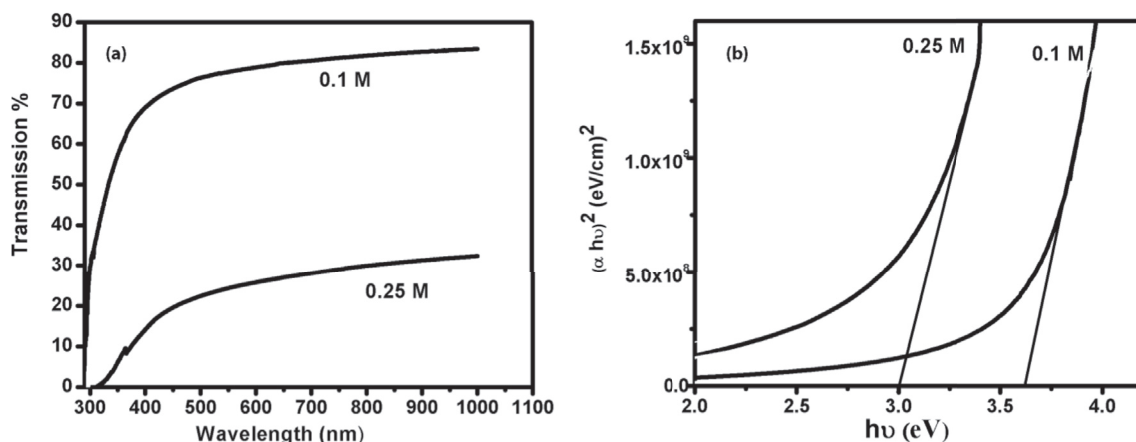


**Fig. 4.** (a) Transmittance spectrum and (b) Tauc plot of SnO thin films for 0.1 M and 0.25 M concentration of precursor solutions.

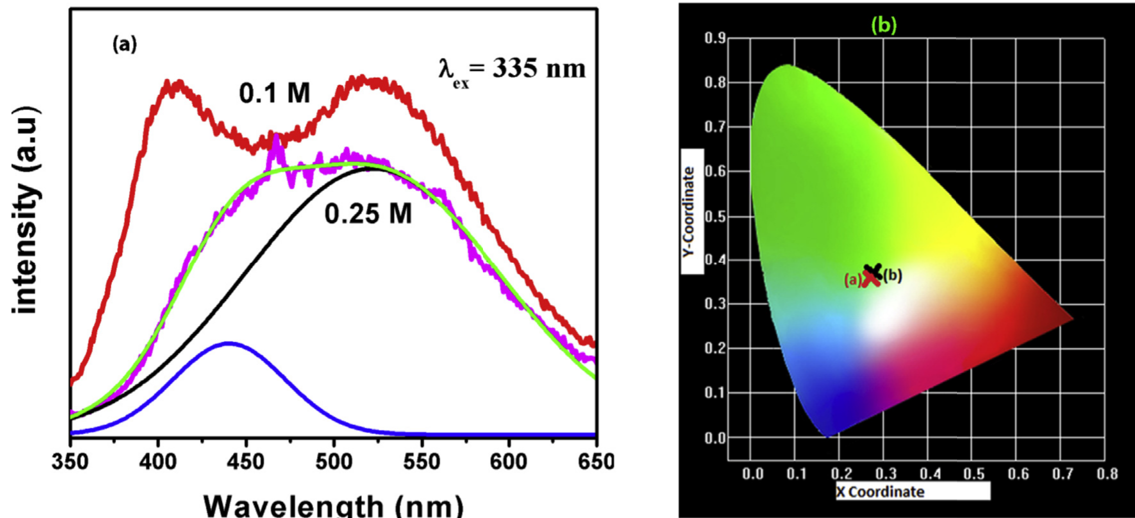


**Fig. 5.** (a) PL spectra and (b) CIE diagram of SnO thin films for 0.1 M and 0.25 M concentration of precursor solutions.

oxygen vacancies are present which may be the reason for DLE emission in SnO thin films at 520 nm.

The chromaticity coordinates (x, y) were calculated using the Commission Internationale del'Eclairage (CIE) coordinate calculator from the emission spectrum [28]. The colour coordinates for SnO thin films in the CIE chromaticity diagram is shown in Fig. 5(b) by a solid cross(X). From Fig. 5(b), green emission is observed for both the samples with CIE coordinates $x = 0.281, y = 0.371$ and $x = 0.278, y = 0.369$ respectively for 0.1 M and 0.25 M SnO thin films.

### 3.6. Ellipsometric analysis

Three kinds of unknown quantities like film thickness, the real part of the refractive index (n) and the imaginary part (extinction coefficient k) determined by ellipsometric technique. The use of ellipsometric technique depends on the choice of the angle of incidence (ϕ) and wavelength (λ). So in order to determine the unknown quantities, it was desirable to find a suitable region of spectral range and angle of incidence. The ellipsometric parameters Ψ and Δ are defined by Ref. [29].

$$\tan\psi = |R_p|/|R_s|\&$$

$$\Delta = \Delta_p - \Delta_s$$

where

$R_p = |R_p| \exp(I\Delta_p)$
& $R_s = |R_s| \exp(I\Delta_s)$ are the complex Fresnel reflection coefficients for p and s polarized pairs respectively.

Ψ and Δ were acquired at angle of incidence (ϕ) 55° over the spectral range 200–1000 nm in steps of 100 nm. The mean square error (MSE) was the evaluation of the match quality between measurement (exp) & model data (mod) and was defined according to the Levenberg-Marquardt algorithm as [30].

$$MSE = \frac{1}{2N - M}\sum_{i=1}^{N}\left[\left(\frac{\psi_i^{mod} - \psi_i^{exp}}{\sigma_{\psi_i}^{exp}}\right)^2 + \left(\frac{\Delta_i^{mod} - \Delta_i^{exp}}{\sigma_{\Delta_i}^{exp}}\right)^2\right]$$

where N was the number of measured Ψ and Δ pairs, M was the total number of real valued fitting parameters and $\sigma_\Psi$ & $\sigma_\Delta$ were the standard deviations on the experimental data. It was required that $2N \geq M$ and minimize the MSE (<10).

The thickness of the SnO films is obtained as 86 nm and 134 nm respectively for 0.1 M and 0.25 M precursor concentrations. The refractive index of the film for 632.8 nm was found to be ~1.72 (0.1 M) and 1.83 (0.25 M) respectively. Table 1 shows the Ellipsometric data obtained for 0.1 M and 0.25 M samples respectively. Fig. 6(a and b) shows the variation of refractive index and extinction coefficient with wavelength for 0.1 M and 0.25 M SnO thin film samples.

From Fig. 6(a), it was observed that for 0.1 M sample, the refractive index (n) decreases with wavelength in the visible range and the refractive index slightly increases at the IR range. Conversely, for the films deposited with 0.25 M concentration of the precursor solution, the refractive index increases with wavelength in the visible range and it decreases with wavelength in the IR range. The refractive index of 0.1 M sample is 1.72 and 0.25 M sample is 1.84. The variation of refractive index of the samples is due to the variation in oxygen content of the deposited films. From Fig. 6(b), it was observed that the extinction coefficient (k) decreases with wavelength for both the samples. Interestingly, the refractive index and extinction coefficient have opposite behaviour. From Fig. 7(a), it was observed that the psi (Ψ) angle decrease with wavelength for 0.25 M sample, and for 0.1 M SnO thin film sample first Ψ angle first decreases with wavelength and then increases with wavelength. From Fig. 7(b), it was observed that the delta(Δ) angle for 0.1 M sample decreases with wavelength and from 700 nm the Δ angle is increases with wavelength. For 0.25 M sample, the Δ angle first increases with wavelength and from 500 nm the Δ angle is decreases with wavelength.

### 3.7. Electrical studies

To characterize the electrical properties of the thin films, Hall probe measurements in a van der pauw configuration at room temperature were employed. The SnO films exhibited p-type conduction with the mobility, hole concentration, and the resistivity values as shown in

**Table 1**
Ellipsometric datas of SnO thin films for 0.1 M and 0.25 M concentration of precursor solutions.

| Molarity(M) | Thickness of the film(nm) | Roughness of the film (nm) | Mean Square Error(MSE) | Refractive index (n) at 632.8 nm | Extinction Coefficient(k) at 632.8 nm |
|---|---|---|---|---|---|
| 0.1 | 85.77 | 3.71 | 4.847 | 1.72015 | 0.13899 |
| 0.25 | 134 | 10.30 | 15.335 | 1.83623 | 0.00326 |

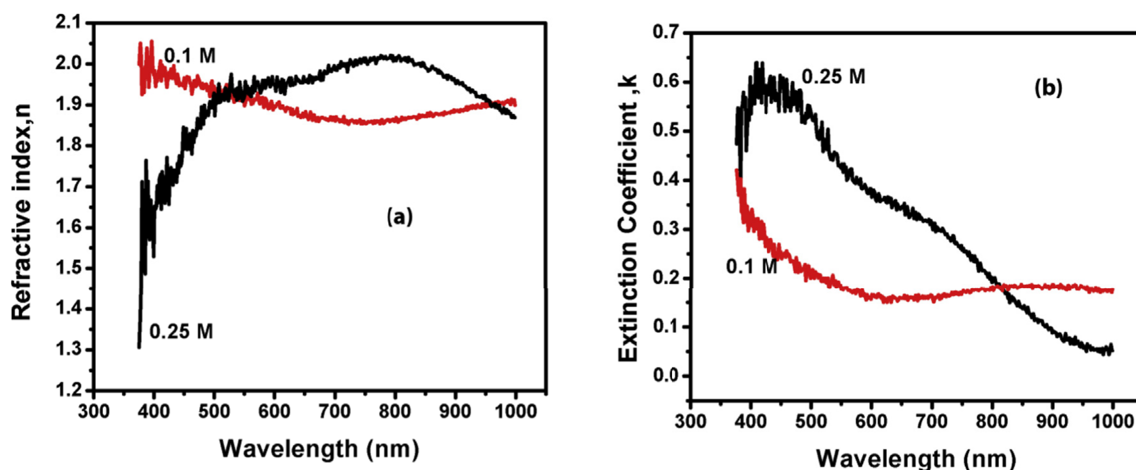


**Fig. 6.** Variation of (a) Refractive index and (b) Extinction Coefficient with Wavelength for 0.1 M and 0.25 M SnO thin films.

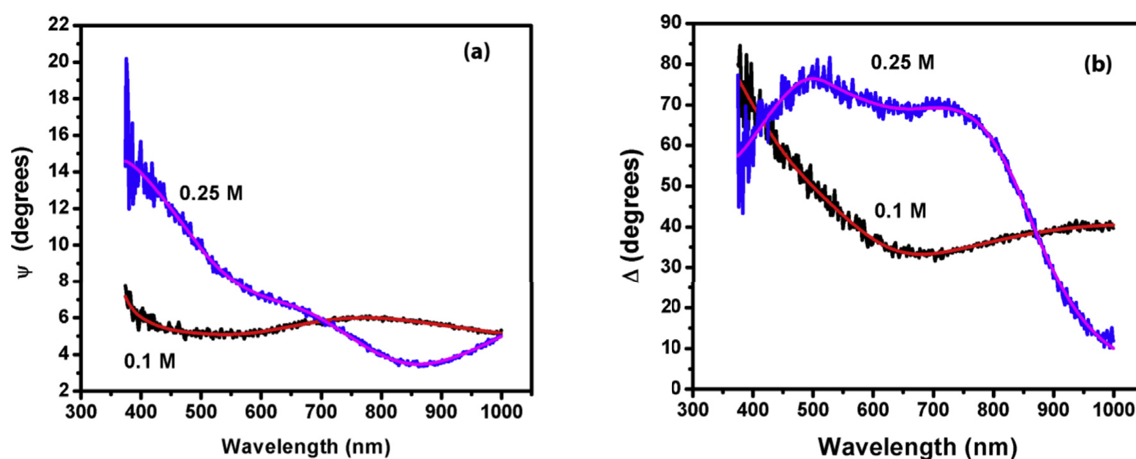


**Fig. 7.** The variation of (a) psi and (b) delta angles with wavelength for 0.1 M & 0.25 M SnO thin films.

Table 2. The change in conductivity is due to both changes in carrier concentration as well as the mobility. According to first-principle calculations, the p-type conductivity of SnO films originated from the oxygen interstitial or/and tin vacancy [10]. The reason for p-type conductivity in our study may be due to interstitial oxygen present in the SnO lattice. SnO has a large hole mobility owing to its hybridized orbitals. In SnO, Sn 5s and O 2p orbitals have nearly equal contribution at its VBM also leading to a p type conductivity [10]. High hole mobility is observed in SnO films deposited in a Sn-rich environment. Increase in hole mobility is due to the presence of metallic β-Sn [15]. From Fig 8(b), presence of metallic tin was confirmed in the SnO thin film sample prepared with 0.25 M precursor concentration. So the mobility of SnO thin film with 0.25 M concentration of the precursor solution have high hole mobility.

In order to study the mechanisms of conductivity, it is convenient to plot logarithm of the conductivity (lnσ) as a function of 1000/T. Fig. 8(a and b) shows the relation between of lnσ versus 1000/T for SnO thin films for different molarities in the range (325-420) K. The activation energy can be determined from the slopes of the Arrhenius plot. From Fig. 8(a), it was observed that, 0.1 M concentration of precursor solution is showing a semiconducting behaviour with activation energy

$E_a = 0.0880$ eV. From Fig. 8(b), for 0.25 M concentration of the precursor solution we observe a conducting behaviour with two activation energies $E_{a1} = -0.2632$ eV & $E_{a2} = -0.07912$ eV. The metallic behaviour observed in 0.25 M concentration of precursor solution may be due to metallic tin (β-Sn) present in the film. From Fig. 8(a and b), As the concentration of the precursor solution increases the SnO thin film changes its conducting behaviour from semiconducting to metallic that is due to the increase in concentration of tin (Sn) present in the sample.

## 4. Conclusions

Polycrystalline P- type semiconducting SnO thin films were deposited successfully by chemical spray pyrolysis method at 350 °C for 0.1 M and 0.25 M concentrations of precursor solutions. XRD studies show that the films grown are of orthorhombic crystal structure. The XRD and SEM studies reveals that the average grain size was increases with molarity. Among the two samples, the sample grown with 0.1 M precursor solution

**Table 2**
Electrical studies of SnO thin films.

| Molarity (M) | Carrier Concentration (/cm$^3$) | Resistivity (Ω cm) | Conductivity (Siemens/cm) | Mobility (cm$^2$/V sec) | Thickness (nm) | Avg.Hall coefficient (cm$^3$/C) | Conductivity Type |
|---|---|---|---|---|---|---|---|
| 0.1 | $6.8 \times 10^{18}$ | $1.2 \times 10^{-1}$ | 8.5 | 7.8 | 86 | $9.2 \times 10^{-1}$ | P |
| 0.25 | $7.1 \times 10^{18}$ | $5.9 \times 10^{-2}$ | 17.1 | 15 | 134 | $8.8 \times 10^{-1}$ | P |

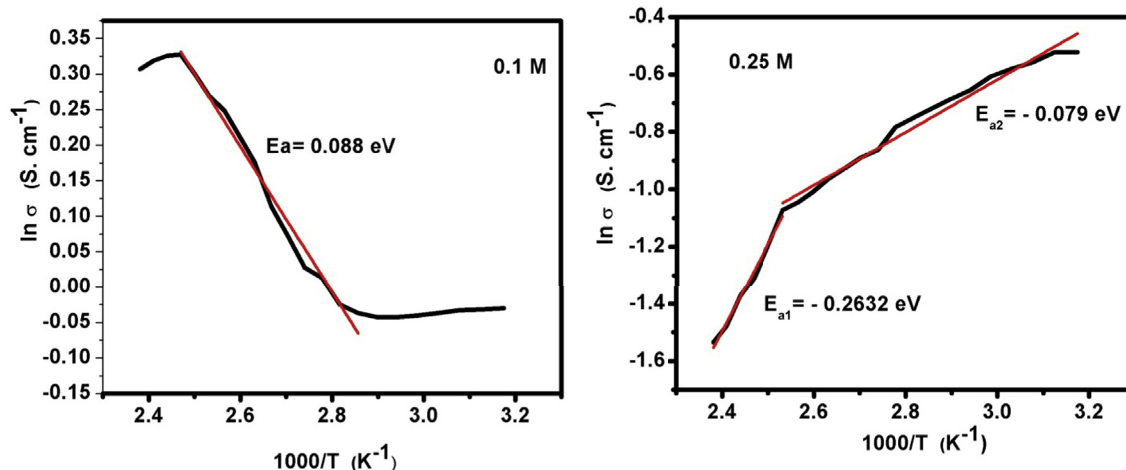


**Fig. 8.** Arrhenius plot of SnO thin films for (a) 0.1 M and (b) 0.25 M concentration of precursor solutions.

is highly transparent (82%) with a wide band gap of 3.58 eV. The hole concentration in the sample is $6.8 \times 10^{18}$ $cm^{-3}$and it has a high hole mobility of 7.8 $cm^2V^{-1}s^{-1}$ making it applicable in the fabrication of p-type thin film transistors and other optoelectronic devices. EDX analysis confirms the presence of Sn and O elements in the prepared SnO thin film. The thickness, refractive index, extinction coefficients were obtained by ellipsometric technique. As the nature of this process is inherently low-cost, this work may be a platform to prepare p-type SnO thin films using a simple and reproducible method for future research.

## Acknowledgement

The authors gratefully acknowledges Sophisticated Analytical Instrument Facility (SAIF), IIT Bombay for SEM measurements. Authors thank Board of Research in Nuclear Sciences (BRNS), Department of Atomic Energy (DAE) for supporting this work through project 34/14/58/2014-BRNS.

## References

[1] M. Oshima, K. Yoshino, J. Electron. Mater. 39 (2010) 819.
[2] A.V. Moholkar, S.M. Pawar, K.Y. Rajpure, C.H. Bhoshale, J.H. Kim, Appl. Surf. Sci. 255 (2009) 9358.
[3] J. Ouerfelli, S.O. Djobo, J.C. Bernede, L. Cattin, M. Morsliy, Y. Berredjem, Mater. Chem. Phys. 112 (2008) 198.
[4] F. Gu, S.F. Wang, M.K. Lu, Y.X. Qi, G.J. Zhou, D. Xu, Dir Yoan, Opt. Mater. 25 (2004) 59.
[5] A.A. Firooz, A.R. Mahjoub, A.A. Khodadai, Sens. Actuators B Chem. 141 (2009) 89.
[6] R.M. Agrawal, J. Electron Devices 12 (2012) 730.
[7] V. Subramanian, K. Gnanasekar, B. Rambabu, Solid State Ionics 175 (2004), 181184.
[8] V. Shrotriya, G. Li, Y. Yao, C.-W. Chu, Y. Yang, Appl. Phys. Lett. 88 (2006), 073508.
[9] W. Guo, Fu L. Zhang, Y. Zhang, L.Y. Liang, Z.M. Liu, H.T. Cao, X.Q. Pan, Appl. Phys. Lett. 96 (2010), 042113.
[10] A. Togo, F. Oba, I. Tanaka, Phys. Rev. B 74 (2006), 195128.
[11] R. Sivaramasubramaniam, R. Muhamad, S. Radhakrishn, Phys. Status Solidi. A 136 (1993) 215.
[12] J.J. Ning, T. Jiang, K.K. Men, Q.Q. Dai, D.M. Li, Y.J. Wei, et al., J. Phys Chem. C 113 (2009) 14140.
[13] Y. Ogo, H. Hiramatsu, K. Nomura, H. Yanagi, T. Kamiya, M. Kimura, M. Hirano, H. Hosono, Phys. Status Solidi A 206 (2009) 2187.
[14] K.C. Sanal, M.K. Jayaraj, Mater. Sci. Eng. B 178 (2013) 816.
[15] E. Fortunato, R. Barros, P. Barquinha, V. Figueiredo, S.H.K. Park, Appl. Phys. Lett. 97 (2010), 052105.
[16] Y. Ogo, H. Hiramatsu, K. Nomura, H. Yanagi, T. Kamiya, M. Hirano, et al., Appl. Phys. Lett. 93 (2008), 032113.
[17] L.Y. Liang, Z.M. Liu, H.T. Cao, X.Q. Pan, ACS Appl. Mater Interf. 2 (2010) 1060.
[18] Jesus A. Caraveo-Frescas, Pradipta K. Nayak, Hala A. Al-Jawhari, Danilo B. Granato, Udo Schwingenschlögl, Husam N. Alshareef, ACS Nano 7 (2013) 5160.
[19] H. Yabuta, N. Kaji, R. Hayashi, H. Kumomi, K. Nomura, T. Kamiya, et al., Appl. Phys. Lett. 97 (2010), 072111.
[20] M. Marikkannan, V. Vishnukanthan, A. Vijayshankar, J. Mayandi, J.M. Pearce, AIP Adv. 5 (2015), 027122.
[21] X. Du, Y. Du, S.M. George, J. VacSci Technol. A 23 (2005) 581.
[22] H. Hosono, Y. Ogo, H. Yanagi, T. Kamiya, ElectrochemSolid-StateLett 14 (2011) 13.
[23] M. Karunakaran, S. Maheswari, K. Kasirajan, S. Dineshraj, IJRASET 4 (7) (2016) 2321–9653.
[24] T.A. Safeera, N. Johns, E.I. Anila, Arturo I. Martinez, P.V. Sreenivasan, R. Reshmi, Mallick Sudhanshu, M.K. Jayaraj, J. Anal. Appl. Pyrolysis 115 (2015) 96.
[25] W.H. Hall, G.K. Williamson, The diffraction pattern of cold worked metals: I the nature of extinction, in: Proceedings of the Physical Society (SectionB-64), West Midlands, United Kingdom, 1951, pp. 937–946.
[26] G.K. Williamson, W.H. Hall, X-ray line broadening from filed aluminium and wolfram, Acta Metall. 1 (1953) 22–31.
[27] Tui Zeng, Chang-Dong Gu, Xi-Li Wang, Jiang-Ping Tu, J. Nanoparticle Res. 16 (2014) 2288.
[28] P.R. Boyce, Human Factors in Lighting, second ed., Taylor and Francis Inc., New York, 2003.
[29] A. Kalnitsky, S.P. Tay, J.P. Ellul, S. Chongsawangvirod, J.W. Andrews, E.A. Irene, J. Electrochem. Soc. 137 (1990) 234.
[30] Woollam, J.A. Co., Inc.; Guide to using WVASE32 software for optical data analysis.